Direct Measurement of Metal Ion Chelation in the Active Site of Human Ferrochelatase[†]

M. Hoggins,[‡] H. A. Dailey,[§] C. N. Hunter,[‡] and J. D. Reid*,[‖]

Department of Molecular Biology and Biotechnology, University of Sheffield, Sheffield, U.K. S10 2TN, Biomedical and Health Sciences Institute, Paul D. Coverdell Center, University of Georgia, Athens, Georgia 30602-7394, and Department of Chemistry, University of Sheffield, Sheffield, U.K. S3 7HF

Received November 22, 2006; Revised Manuscript Received May 1, 2007

ABSTRACT: The final step in heme biosynthesis, insertion of ferrous iron into protoporphyrin IX, is catalyzed by protoporphyrin IX ferrochelatase (EC 4.99.1.1). We demonstrate that pre-steady state human ferrochelatase (R115L) exhibits a stoichiometric burst of product formation and substrate consumption, consistent with a rate-determining step following metal ion chelation. Detailed analysis shows that chelation requires at least two steps, rapid binding followed by a slower ($k \approx 1$ s^{-1}) irreversible step, provisionally assigned to metal ion chelation. Comparison with steady state data reveals that the rate-determining step in the overall reaction, conversion of free porphyrin to free metalloporphyrin, occurs after chelation and is most probably product release. We have measured rate constants for significant steps on the enzyme and demonstrate that metal ion chelation, with a rate constant of 0.96 s^{-1}, is ∼10 times faster than the rate-determining step in the steady state ($k_{cat} = 0.1$ s^{-1}). The effect of an additional E343D mutation is apparent at multiple stages in the reaction cycle with a 7-fold decrease in k_{cat} and a 3-fold decrease in k_{chel}. This conservative mutation primarily affects events occurring after metal ion chelation. Further evaluation of structure−function data on site-directed mutants will therefore require both steady state and pre-steady state approaches.

The final step in heme biosynthesis, insertion of ferrous iron into protoporphyrin IX, is catalyzed by protoporphyrin IX ferrochelatase (protoheme ferro-lyase, EC 4.99.1.1; the human enzyme is hereafter called ferrochelatase). The mechanisms of biological iron chelation have proven to be of great interest with a range of studies examining reaction kinetics (*1*−*3*), spectroscopy of bound intermediates (*4*−*6*), sensitivity of the reaction to structural variation (*1*, *3*), and behavior of the enzyme analogues, including antibodies (*4*, *7*−*9*) and both DNA and RNA (*10*−*12*) that also catalyze insertion of metal ion into porphyrins. Additionally, crystal structures of free enzyme (*13*, *14*), as well as with bound metal substrate, bound porphyrin substrate (*15*), and a tight-binding competitive inhibitor (*16*) should support confident interpretation of the link between structure and function in this system. In fact, controversy remains over the role of individual residues in the reaction mechanism. Compare, for example, the suggested metal ion binding site of Sellers et al. (*1*) with that proposed by Gora et al. (*17*); a recent review provides a fair summary (*18*). In part, this difficulty arises when the functional significance of individual residues is assessed on the basis of steady state kinetic parameters which generally reflect multiple reaction steps as well as assignment of putative catalytically significant residues on the basis of an incorrect assumption that the *N*-alkyl porphyrin inhibitor binds in the same site and orientation as the native protoporphyrin substrate. Our development of a transient kinetic approach to monitoring individual reaction steps should help resolve the mechanistic details of this system.

The in vivo delivery of substrates to ferrochelatase is an area of much current activity with recent proposals suggesting a role for chaperones and for substrate channeling. The porphyrin substrate, protoporphyrin IX, is synthesized from protoporphyrinogen IX in a six-electron oxidation. The enzyme, protoporphyrinogen oxidase (PPO,[1] EC 1.3.3.4), is associated with the periplasmic side of the inner mitochondrial membrane, i.e., the opposite side of the membrane from ferrochelatase (*19*). A recent report on the crystal structure of a plant PPO reported that the membrane-associated face of this enzyme is complementary to that of ferrochelatase (*20*). This was in accord with previous studies that suggested the two enzymes form a complex and that, in eukaryotic systems at least, protoporphyrin IX is channeled to ferrochelatase across the inner mitochondrial membrane (*20*, *21*). It has also been proposed that iron is transported directly to ferrochelatase from the inner mitochondrial membrane (*22*, *23*), although an alternative theory suggests that ferrous iron is transferred to ferrochelatase from frataxin, a putative mitochondrial iron chaperone (*24*).

[†] Funded by the BBSRC (U.K.).

* To whom correspondence should be addressed: Department of Chemistry, University of Sheffield, Sheffield, U.K. S3 7HF. Telephone: +44 114 222 29558. Fax: +44 114 222 9346. E-mail: j.reid@sheffield.ac.uk.

[‡] Department of Molecular Biology and Biotechnology, University of Sheffield.

[§] University of Georgia.

[‖] Department of Chemistry, University of Sheffield.

[1] Abbreviations: PPO, protoporphyrinogen oxidase; DIX, deuteroporphyrin IX.

10.1021/bi602418e CCC: $37.00
Published on Web 06/13/2007

Chelatases catalyze porphyrin metalation by stabilizing a deformed porphyrin intermediate; this conclusion arises from a series of experimental data, including resonance Raman spectroscopy of bound porphyrins (*4*, *5*), cocrystallization of the nonplanar *N*-methyl mesoporphyrin with the ferrochelatase from *Bacillus subtilis* (*16*), and the use of nonplanar porphyrins in generating model catalysts, including both antibodies (*4*, *7*−*9*) and nucleic acids (*10*−*12*). Recent theoretical calculations also support this conclusion (*25*, *26*), as does the crystal structure of human ferrochelatase with a bound protoporphyrin substrate (*18*). On the basis of a comparison of the observed rates of insertion of metal ion into a nonplanar substrate analogue with steady state kinetic parameters, porphyrin deformation has recently been proposed to be the key event in determining the metal ion specificity of a particular metal ion chelatase (*18*).

A considerable number of papers describe the steady state behavior of ferrochelatase (e.g., refs *1*−*3*), but there are very few reports of transient kinetics (*3*, *27*). Most functional analysis and assessment of the significance of mutated residues has relied on steady state information. As ferrochelatase catalyzes the biologically critical conversion of a highly absorbing and fluorescent porphyrin into a nonfluorescent metalloporphyrin with a distinct absorbance spectrum, this enzyme is amenable to transient kinetic analyses (*1*). We have exploited the large optical signal associated with metal chelation in directly assessing catalytic events in the active site of ferrochelatase.

MATERIALS AND METHODS

Materials. Unless otherwise stated, chemicals were obtained from Sigma Chemical Co. (Poole, Dorset, U.K.).

Enzyme Purification. Recombinant human ferrochelatase (R115L) was purified essentially as described previously (*28*). Briefly, *Escherichia coli* JM109 cells containing recombinant ferrochelatase were suspended in solubilization buffer [50 mM TRIS-MOPS, 0.1 M KCl, and 1% (w/v) sodium cholate (pH 8.0)] containing 1 mM 4-(2-aminoethyl)-benzenesulfonyl fluoride, sonicated on ice for 3 × 30 s, and centrifuged at 50000*g* for 30 min at 4 °C. The supernatant was loaded onto a 2 mL Talon column (Clontech, Palo Alto, CA), previously equilibrated with solubilization buffer. The column was washed with 20 mL of solubilization buffer, and 10 mL of solubolization buffer containing in addition 1 M KCl. Ferrochelatase was eluted with solubilization buffer containing 300 mM imidazole. The column wash containing 1 M KCl was used to remove any endogenous porphyrin. Imidazole was removed by applying purified protein to a 40 mL column of P-6DG (Bio-Rad, Hemel Hempstead, U.K.) equilibrated in solubilization buffer. Pure protein was stored under liquid N_2 in 50 mM TRIS-MOPS, 0.1 M KCl, and 1% (w/v) sodium cholate (pH 8.0). The protein concentration was determined spectrophotometrically using the calculated extinction coefficient ϵ_{278} of 46 900 M^{-1} cm^{-1} (*28*).

Enzyme Assays. Steady state rates of metal ion insertion were determined using ferrous iron and deuteroporphyrin IX (Porphyrin Products, Logan, UT) as substrates in a spectrophotometric assay (*1*, *29*) with 0.17 μM active R115L ferrochelatase (determined by active site titration, 0.19 μM total enzyme) or with 0.16 μM active R115L/E343D ferrochelatase (determined by active site titration, 0.19 μM total enzyme). Reactions were carried out in 100 mM TRIS-HCl, 0.5% Tween 20, and 1 mM β-mercaptoethanol (pH 8.1) and at 30 °C. Steady state kinetic parameters were evaluated by fitting eq 1 to the initial rates using nonlinear regression analysis implemented in Igor Pro (Wavemetrics Inc., Lake Oswego, OR). Values of k_{cat} and k_{cat}/K_m were estimated using the concentration of active enzyme derived from the active site titration described below.

$$v_i = \frac{V}{1 + \frac{K_m^{D_{IX}}}{[D_{IX}]} + \frac{K_m^{Fe}}{[Fe]} + \frac{K^{D_{IX}\cdot Fe}}{[D_{IX}][Fe]}} \quad (1)$$

Transient kinetic studies were performed on an Applied Photophysics Pi-star spectrophotometer with a 2 mm light path operating in fluorescence mode or a 10 mm light path operating in absorbance mode. To detect substrate fluorescence, excitation light from a xenon source passed through a monochromator set at 496 nm, and emitted light was detected at 90° through a 515 nm cutoff filter (OG515, Schott). Absorbance traces were recorded at either 496 nm, measuring substrate depletion, or 548 nm, measuring the level of accumulation of product. Traces were collected under the conditions described above for steady state kinetics. Averaged traces ($n \geq 6$) were evaluated by fitting the time course to eq 2

$$[P]_t = Ae^{-k_{obs}t} + v_i t \quad (2)$$

which describes a pre-steady state burst phase, with amplitude A and an observed rate constant k_{obs}, followed by a linear steady state conversion of substrate into product characterized by a steady state rate, v_i, using the data analysis software (ProData 1.43, Applied Photophysics, Leatherhead, Surrey, U.K.) supplied with the instrument. The burst amplitude is proportional to the concentration of intact active sites provided that the rate constant for the burst is sufficiently greater than the rate constant for the subsequent step (*30*). This relationship was used to estimate the concentration of an enzyme preparation in terms of active sites.

RESULTS

Human ferrochelatase can be readily overexpressed and purified using established methods. This ferrochelatase (R115L) shows steady state kinetic behavior and activity (Figure 1) similar to those seen previously (*1*). Steady state kinetic parameters were obtained by a global fit to eq 1. The apparent kinetic parameters obtained from individual v_i versus [S] curves show good agreement with the theoretical curves calculated from the global fit (Figure 2). The R115L ferrochelatase mutant increases stability without a significant impact on enzyme activity (*28*); a crystal structure of this mutant is available [PDB entry 1HRK (*13*)]. The R115L/E343D double mutant has a k_{cat} substantially lower than that of the R115L mutant, but they have similar K_m values (*1*). In both cases, purification using previously described methods (*28*) yields protein with a small amount of bound porphyrin, which was removed by incorporating a high-salt wash (1 M KCl) into the purification procedure. This is an essential step as adventitious porphyrin reduces the concen-

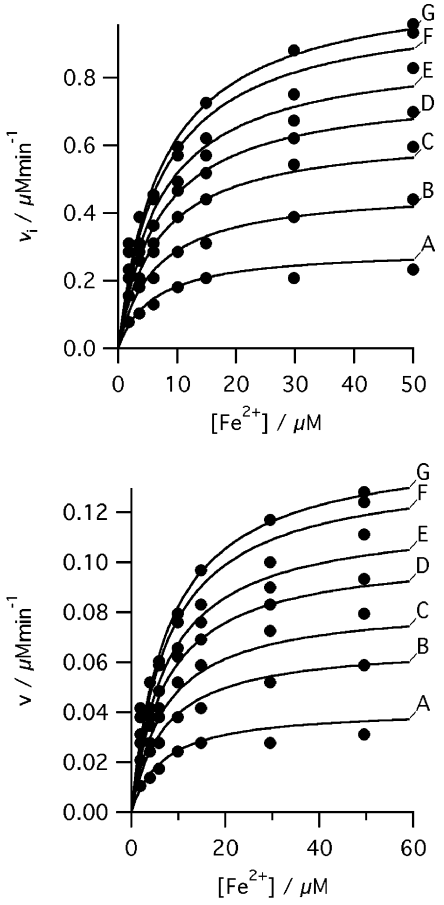

FIGURE 1: Initial rates of ferrochelatase-catalyzed insertion of iron into deuteroporphyrin at pH 8.1 in 100 mM TRIS-HCl, 250 μM Fe^{2+}, 1 mM β-mercaptoethanol, and 0.5% (v/v) Tween 20 at 30 °C. In the top panel, with 0.17 μM R115L ferrochelatase, deuteroporphyrin concentrations were (A) 1.8, (B) 3.6, (C) 6.3, (D) 9.9, (E) 15.3, (F) 29.7, and (G) 49.6 μM. The points are experimental, and the theoretical lines are described by eq 1 with the following characteristic parameters: $K_m^{Fe} = 7.7 \pm 1.4$ μM, $K_m^{D_{IX}} = 5.5 \pm 0.5$ μM, $K^{Fe\cdot D_{IX}} = 30.54 \pm 8.01$ μM^2, and $V = 1.21$ μM/min. In the bottom panel, with 0.16 μM R115L/E343D ferrochelatase, deuteroporphyrin concentrations were (A) 1.9, (B) 4.0, (C) 5.9, (D) 9.9, (E) 14.9, (F) 29.7, and (G) 49.7 μM. The points are experimental, and the theoretical lines are described by eq 1 with the following characteristic parameters: $K_m^{Fe} = 8.2 \pm 1.0$ μM, $K_m^{D_{IX}} = 5.8 \pm 0.8$ μM, $K^{Fe\cdot D_{IX}} = 34.8 \pm 8.3$ μM^2, and $V = 0.16 \pm 0.01$ μM/min.

tration of available enzyme active sites and thus the observable amplitude of the pre-steady state transient.

A pre-steady state burst phase was measured using either stopped-flow absorbance (data not shown) or fluorescence spectroscopy (Figure 3). The fluorescence measurements monitored substrate consumption. Amplitudes of product formation and substrate consumption were quantified from the absorbance data. Shifts in porphyrin spectra on ferrochelatase binding have been described previously (*31*) and could potentially interfere with a spectroscopic active site titration. In this case, as the enzyme−porphyrin complex does not accumulate, the burst in substrate consumption arises from the loss of free substrate and can be accurately quantified. Additionally, as amplitudes of substrate consumption and product formation at 548 nm agree closely, there is little difference between the extinction coefficients of bound and free product. The amplitude of the burst in product formation was calculated to correspond to 90% of the total

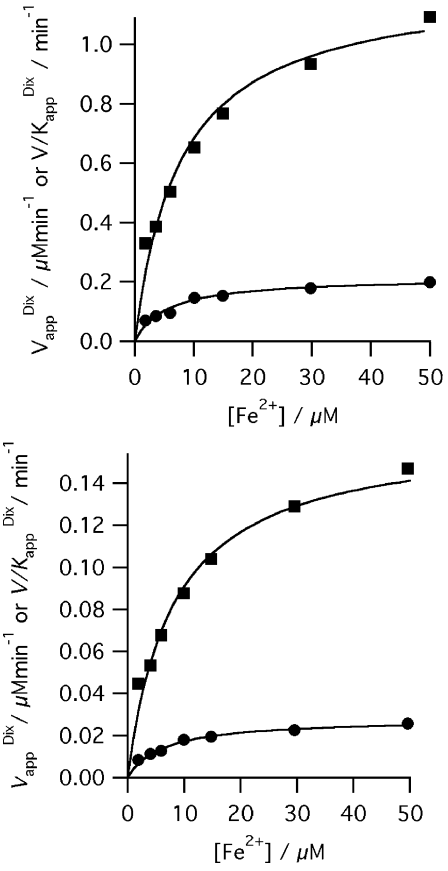

FIGURE 2: Secondary plots showing the iron dependence of the observed kinetic parameters. The points are the apparent kinetic parameters that arise from fitting the Michaelis−Menten equation to individual v_i vs [S] curves, and the lines are described by eq 1 [V_{app} (■) and V/K_{app} (●)] with the following characteristic parameters: (top) for R115L ferrochelatase, $K_m^{Fe} = 7.7 \pm 1.4$ μM, $K_m^{D_{IX}} = 5.5 \pm 0.5$ μM, $K^{Fe\cdot D_{IX}} = 30.54 \pm 8.01$ μM^2, and $V = 1.21$ μM/min, and (bottom) for R115L/E343D ferrochelatase, $K_m^{Fe} = 8.2 \pm 1.0$ μM, $K_m^{D_{IX}} = 5.8 \pm 0.8$ μM, $K^{Fe\cdot D_{IX}} = 34.8 \pm 8.3$ μM^2, and $V = 0.16 \pm 0.01$ μM/min.

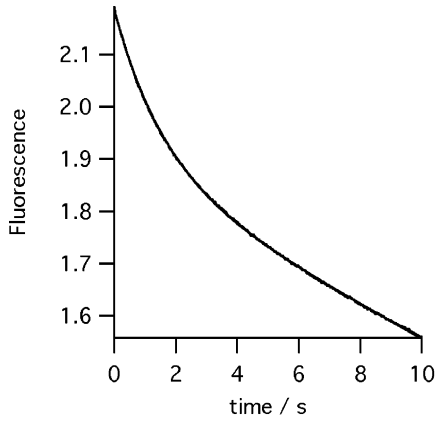

FIGURE 3: Time course of consumption of D_{IX} (25 μM) by ferrochelatase (0.5 μM) at pH 8.1 in 100 mM TRIS-HCl, 250 μM Fe^{2+}, 1 mM β-mercaptoethanol, and 0.5% (v/v) Tween 20 at 30 °C.

enzyme concentration. This relationship holds as the concentration of ferrochelatase is varied from 0.5 to 5 μM.

The burst in metalloporphyrin formation allows us to directly assess insertion of metal ion into the porphyrin ring. Progress curves can be described by a single-exponential phase followed by a linear steady state conversion of

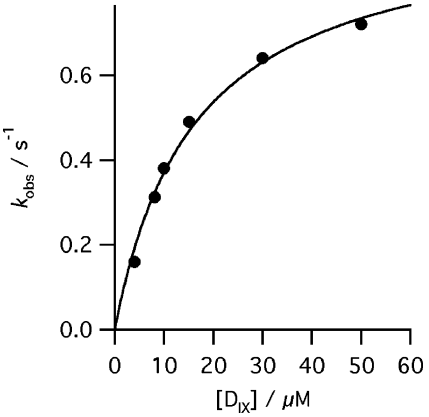

FIGURE 4: Dependence of k_{obs} for the reaction of R115L human ferrochelatase (0.5 μM) on deuteroporphyrin concentration at pH 8.1 in 100 mM TRIS-HCl, 250 μM Fe^{2+}, 1 mM β-mercaptoethanol, and 0.5% (v/v) Tween 20 at 30 °C. The points are experimental, and the theoretical line is described by eq 3 and the following characteristic parameters: $k_{chel} = 0.97 \pm 0.05$ s^{-1}, and $K_s^{D_{IX}} = 16.3 \pm 1.9$ μM.

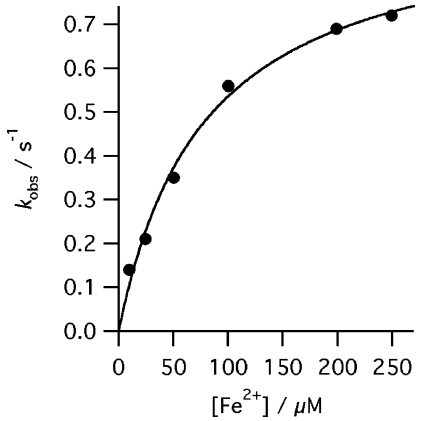

FIGURE 5: Dependence of k_{obs} for the reaction of R115L human ferrochelatase (0.5 μM) on Fe^{2+} concentration at pH 8.1 in 100 mM TRIS-HCl, 50 μM D_{IX}, 1 mM β-mercaptoethanol, and 0.5% (v/v) Tween 20 at 30 °C. The points are experimental, and the theoretical line is described by eq 3 and the following characteristic parameters: $k_{chel} = 0.96 \pm 0.05$ s^{-1}, and $K_s^{Fe} = 79.1 \pm 11.2$ μM.

substrate into product (eq 2). The observed rate constant (k_{obs}) for metal ion insertion catalyzed by R115L ferrochelatase exhibits a hyperbolic dependence on porphyrin concentration with saturating ferrous iron (Figure 4). Similarly, when porphyrin is at a saturating level, the observed rate constant shows a hyperbolic dependence on the concentration of ferrous iron (Figure 5). The R115L/E343D mutant also exhibits similar hyperbolic concentration dependencies on porphyrin (Figure 6) and ferrous iron concentrations (Figure 7). These behaviors are characteristic of a two-step mechanism with rapid substrate binding followed by a slower step, in this case metal ion chelation (Scheme 1). The relationship between the observed rate constant, k_{obs}, and substrate concentration (eq 3) predicts a positive ordinal intercept if the rate constant for on-enzyme dechelation is significant. This is not observed, so the on-enzyme metal ion chelation can be treated as irreversible.

$$k_{obs} = \frac{k_{+2}}{1 + \frac{K'_m}{[S]}} + k_{-2} \quad (3)$$

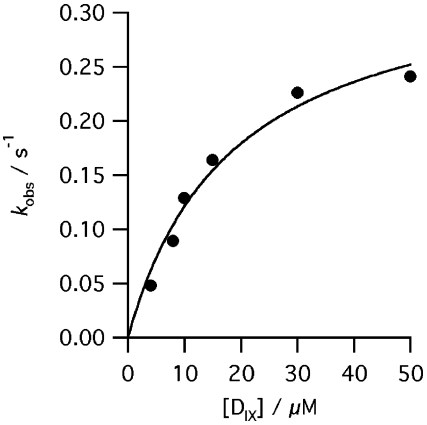

FIGURE 6: Dependence of k_{obs} for the reaction of E343D/R115L human ferrochelatase (0.5 μM) on deuteroporphyrin concentration at pH 8.1 in 100 mM TRIS-HCl, 350 μM Fe^{2+}, 1 mM β-mercaptoethanol, and 0.5% (v/v) Tween 20 at 30 °C. The points are experimental, and the theoretical line is described by eq 3 and the following characteristic parameters: $k_{chel} = 0.35 \pm 0.3$ s^{-1}, and $K_s^{D_{IX}} = 18.6 \pm 4.2$ μM.

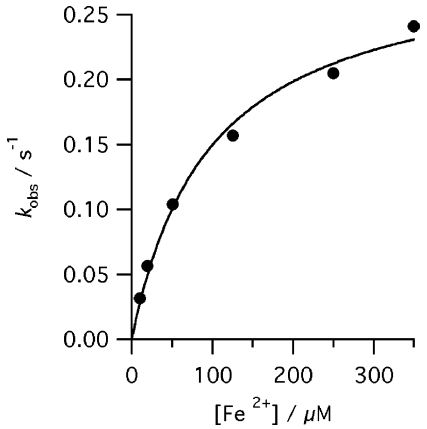

FIGURE 7: Dependence of k_{obs} for the reaction of E343D/R115L human ferrochelatase (0.5 μM) on Fe^{2+} concentration at pH 8.1 in 100 mM TRIS-HCl, 50 μM D_{IX}, 1 mM β-mercaptoethanol, and 0.5% (v/v) Tween 20 at 30 °C. The points are experimental, and the theoretical line is described by eq 3 and the following characteristic parameters: $k_{chel} = 0.30 \pm 0.03$ s^{-1}, and $K_s^{Fe} = 97.6 \pm 15.7$ μM.

Scheme 1: Two-Step Binding of a Substrate (S) to an Enzyme (E)

$$E + S \underset{k_{-1}}{\overset{k_{+1}}{\rightleftharpoons}} ES \underset{k_{-2}}{\overset{k_{+2}}{\rightleftharpoons}} EP$$

where

$$K'_m = \frac{k_{-1} + k_{+2}}{k_{+1}}$$

DISCUSSION

Even though extensive steady state analyses of both wild-type and mutant ferrochelatases are available (*1*), no systematic transient kinetic analysis of the ferrochelatase-catalyzed reaction has been carried out. We therefore investigated the pre-steady state kinetics of the ferrochelatase-catalyzed insertion of ferrous iron into a porphyrin macro-

Scheme 2: Minimal Model for the Ferrochelatase Reaction

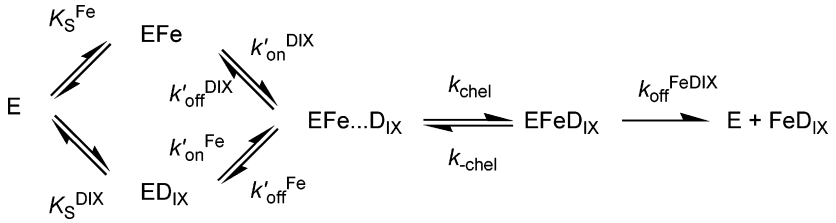

cycle. A mutant ferrochelatase (R115L) with behavior similar to that of the wild type and a double mutant (E343D/R115L) with a substantially reduced k_{cat} were studied. The observed kinetic behavior of both ferrochelatases allowed us to conclude that chelation is not rate-determining in the steady state and that an additional slow step is required for product release. The effect of the additional E343D mutation is apparent at multiple stages in the reaction cycle, emphasizing the benefits available from a transient kinetic analysis of mutant ferrochelatases.

A pre-steady state burst has recently been observed in the murine ferrochelatase-catalyzed insertion of zinc into protoporphyrin IX (*27*); the transient was used to make a detailed study of binding of the inhibitor *N*-methyl protoporphyrin. However, rate constants for insertion of metal ion into the active site were not determined.

The observed burst in formation of product demonstrates that metalloporphyrin formation is fast compared to the rate-determining processes in the steady state. The amplitude of the burst phase, ca. 0.9[E], reveals that in the steady state ferrochelatase exists as an enzyme−product complex. This provides the basis for an active site titration, allowing us to calculate k_{cat} and k_{cat}/K_m for ferrochelatase (*30*, *32*). It is possible that some site-directed mutations will have a deleterious effect on enzyme stability, resulting in an underestimation of steady state kinetic parameters (*33*).

In the case of the steady state data presented in this paper, which benefit from knowledge of the active site concentration, the estimated steady state parameters do not differ substantially from those described previously. This is most probably a result of both the speed of the purification procedure and the stability of the purified material used for steady state analysis (*1*). A recent study revealed that active site mutations can stabilize a series of mutant and wild-type murine ferrochelatases, although this effect may, at least in part, arise from binding to endogenous porphyrin (*33*).

This paper presents the first determination of the steady state kinetic parameters k_{cat}, $k_{cat}/K_m^{D_{IX}}$, and k_{cat}/K_m^{Fe} for any ferrochelatase based on accurate knowledge of the active enzyme concentration. This allows us to compare rate constants for active site chemistry (k_{chel}) and for the overall reaction (k_{cat}); without this information, it could be argued that the fact that k_{chel} is greater than k_{cat} was solely due to an overestimation of the active enzyme concentration.

The substrate dependence of k_{obs} allows us to determine k_{+2} to be 0.96 ± 0.05 s^{-1} in the case of R115L ferrochelatase (Figures 4 and 5) and ca. 0.3 s^{-1} with the E343D mutation (Figures 6 and 7). This is either the rate constant for metal ion chelation or that of a rapid isomerization concomitant with the chelation reaction. This rate constant is thus a lower limit for the metal ion chelation rate constant. As, in both cases, k_{cat} is much smaller that k_{+2}, another slow step is needed to explain the observed kinetics. We therefore extend our model to include an additional slow step after metal ion insertion (Scheme 2). This step includes product dissociation and may also include a kinetically significant isomerization of an enzyme−deuteroheme complex. This additional step is rate-determining in the steady state, and it is the main contributor to k_{cat} (eq 4).

$$k_{cat} = \frac{k_{chel} k_{off}^{FeD_{IX}}}{k_{chel} + k_{-chel} + k_{off}^{FeD_{IX}}} \quad (4)$$

The rate constant for the on-enzyme dechelation reaction, k_{-chel} in Scheme 2, is negligible in the systems described here. We have included it in our model and our descriptions of steady state parameters for the assessment of mutant ferrochelatases and alternative substrates, where $k_{-chel} \neq 0$ and analysis based on the obvious simplified forms of eqs 4 and 5 would be misleading.

Values of K'_m in Scheme 1 can be estimated from the relationship between the substrate concentration and the observed rate constant for metal ion insertion. These parameters relate to the quasi-equilibrium around the ES complex in Scheme 1 and in some cases (i.e., $k_{+2} \ll k_{-1}$) can approximate to K_s, the disassociation constant for the ES complex. It is worth noting that our estimates of K_m and K'_m are significantly different. This arises from the significant contribution that the EP species makes to K_m but not to K'_m (*32*).

This minimal model for the ferrochelatase-catalyzed insertion of iron into deuteroporphyrin (Scheme 2) is shown, for convenience, with random binding of the two substrates. The possibility of ordered binding, as seen with the bovine enzyme (*2*), does not significantly affect our analysis. It has been suggested that in vivo both substrates are channeled to ferrochelatase (*20*−*24*). Therefore, in vitro studies, carried out without the appropriate partner proteins, may not accurately reflect the sequence of binding events occurring in vivo. In any event, this work is concerned with the behavior of metal ion and porphyrin in the active site of ferrochelatase.

In this model (Scheme 2), we propose that metal ion binding is fast. Previous structural models of metal ion binding have described a multistage process in which metal binds initially in a remote site and then moves to the active site (*34*). This model is consistent with the data presented here provided that transport of iron to the active site has a rate constant much greater than 0.96 s^{-1}.

Using our model, we can determine the significance of the steady state parameters k_{cat} and k_{cat}/K_m. The turnover number, k_{cat}, contains contributions from both chelation and product release (eq 4). The K_m values for both substrates contain contributions from chelation and from product

disassociation; for example, the K_m for D_{IX} with random substrate binding and reversible metal ion chelation is equal to $[k_{chel}k_{off}^{FeD_{IX}} + k'_{off}{}^{D_{IX}}(k_{-chel} + k_{off}^{FeD_{IX}})]/[k'_{on}{}^{D_{IX}}(k_{chel} + k_{-chel} + k_{off}^{FeD_{IX}})]$. These parameters cannot then be used as indicators of substrate binding. This is particularly important for kinetic analysis of mutant enzymes where K_m values have frequently been used for this purpose. The apparent second-order rate constant for conversion of free substrate to product, k_{cat}/K_m (eq 5), is more useful in this regard, as it reflects productive substrate binding (*32*).

$$\frac{k_{cat_{D_{IX}}}}{K_m} = \frac{k'_{on}{}^{D_{IX}} k_{chel} k_{off}^{FeD_{IX}}}{k_{chel}\, k_{off}^{FeD_{IX}} + k'_{off}{}^{D_{IX}} (k_{-chel} + k_{off}^{FeD_{IX}})} \quad (5)$$

The kinetic consequences of the additional E343D mutation are a 7-fold reduction in k_{cat} but very little change in K_m for either substrate (*1*). We show that k_{chel} is significantly reduced (ca. 3-fold), although not to the same extent as k_{cat}, suggesting that this conservative mutation perturbs the role of this residue in product release as well as metal ion chelation. We observe no changes in K'_m, suggesting that this conservative mutation does not perturb substrate binding. Previously, this residue has been suggested to have a role in abstraction of protons from the substrate (*1*) or in metal ion binding (*34*, *35*).

A mutation of the analogous murine residue, E287Q, shows a form of porphyrin distortion different from that of the wild type (*31*). Single turnovers of this mutant and the alanine variant suggest that they bind product more tightly (K_d < 20 μM) than the wild type which has a K_d greater than 30 μM (*3*). The effect of mutations at an analogous position (E264Q/E264V) have been considered in the *B. subtilis* enzyme (*35*). Despite an 80% reduction in activity in the E264Q mutant, zinc binding was not perturbed, while the E264V mutant was inactive, and zinc binding could not be assessed. These results are similar to those described for human ferrochelatase. While the analogous human mutant (E343Q) exhibits no activity, the conservative E343D mutation has a sharply reduced k_{cat} with no change in substrate K_m values (*1*).

Our results are consistent with these observations. We see no significant change in K'_m. This parameter can approximate the dissociation constant for a substrate from the ternary complex. In contrast, the 7-fold decrease in k_{cat} can be attributed to events that occur after metal ion chelation. A role in product release for this residue has previously been inferred (*1*, *3*). Additionally, the E343D mutation lowers k_{chel}, disrupting the steps that lead to metal ion chelation. Overall, these results demonstrate that this residue plays a role in multiple steps in the ferrochelatase mechanism. The dual role of this residue is also apparent from the E343K variant which binds and cocrystallizes with porphyrin (*15*), but is inactive (*1*).

In conclusion, we have demonstrated that metal ion chelation is not rate-determining in the catalytic cycle of human ferrochelatase. Therefore, steady state kinetics do not generally provide any information about the significant chemical transformation of the enzyme. In particular, K_m values do not reflect substrate binding and k_{cat} values are dominated by product release. A simple, transient kinetic approach, however, allows us to measure rate constants for significant steps on the enzyme. This approach allows us to demonstrate that metal ion chelation, observed with a rate constant of 0.96 s^{-1}, is at least 10 times faster then the rate-determining step in the steady state (k_{cat} = 0.1 s^{-1}). Evaluation of structure−function data for site-directed mutants therefore requires both steady state and pre-steady state approaches. As an example, the E343D mutant, which displays no alterations in K'_m, nevertheless shows substantial changes in pre-steady state kinetic behavior at multiple reaction steps with a 7-fold decrease in k_{cat} and a 3-fold decrease in k_{chel}. This conservative mutation primarily affects events occurring after metal ion chelation.

REFERENCES

1. Sellers, V. M., Wu, C.-K., Dailey, T. A., and Dailey, H. A. (2001) Human ferrochelatase: Characterization of substrate-iron binding and proton-abstracting residues, *Biochemistry 40*, 9821−9827.
2. Dailey, H. A., and Fleming, J. E. (1983) Bovine ferrochelatase. Kinetic analysis of inhibition by N-methylprotoporphyrin, manganese, and heme, *J. Biol. Chem. 258*, 11453−11459.
3. Franco, R., Pereira, A. S., Tavares, P., Mangravita, A., Barber, M. J., Moura, I., and Ferreira, G. C. (2001) Substitution of murine ferrochelatase glutamate-287 with glutamine or alanine leads to porphyrin substrate-bound variants, *Biochem. J. 356*, 217−222.
4. Romesberg, F. E., Santarsiero, B. D., Spiller, B., Yin, J., Barnes, D., Schultz, P. G., and Stevens, R. C. (1998) Structural and kinetic evidence for strain in biological catalysis, *Biochemistry 37*, 14404−14409.
5. Blackwood, M. E., Jr., Rush, T. S., III, Medlock, A., Dailey, H. A., and Spiro, T. G. (1997) Resonance raman spectra of ferrochelatase reveal porphyrin distortion upon metal binding, *J. Am. Chem. Soc. 119*, 12170−12174.
6. Shi, Z., Franco, R., Haddad, R., Shelnutt, J. A., and Ferreira, G. C. (2006) The Conserved Active-Site Loop Residues of Ferrochelatase Induce Porphyrin Conformational Changes Necessary for Catalysis, *Biochemistry 45*, 2904−2912.
7. Blackwood, M. E., Jr., Rush, T. S., III, Romesberg, F., Schultz, P. G., and Spiro, T. G. (1998) Alternative modes of substrate distortion in enzyme and antibody catalyzed ferrochelation reactions, *Biochemistry 37*, 779−782.
8. Cochran, A. G., and Schultz, P. G. (1990) Antibody-catalyzed porphyrin metallation, *Science 249*, 781−783.
9. Venkateshrao, S., Yin, J., Jarzecki, A. A., Schultz, P. G., and Spiro, T. G. (2004) Porphyrin distortion during affinity maturation of a ferrochelatase antibody, monitored by resonance Raman spectroscopy, *J. Am. Chem. Soc. 126*, 16361−16367.
10. Li, Y., and Sen, D. (1996) A catalytic DNA for porphyrin metallation, *Nat. Struct. Biol. 3*, 743−747.
11. Li, Y., and Sen, D. (1997) Toward an efficient DNAzyme, *Biochemistry 36*, 5589−5599.
12. Conn, M. M., and Schultz, P. G. (1996) Porphyrin Metalation Catalyzed by a Small RNA Molecule, *J. Am. Chem. Soc. 118*, 7012−7013.
13. Wu, C. K., Dailey, H. A., Rose, J. P., Burden, A., Sellers, V. M., and Wang, B. C. (2001) The 2.0 Å structure of human ferrochelatase, the terminal enzyme of heme biosynthesis, *Nat. Struct. Mol. Biol. 8*, 156−160.
14. Al-Karadaghi, S., Hansson, M., Nikonov, S., Jånsson, B., and Hederstedt, L. (1997) Crystal structure of ferrochelatase: The terminal enzyme in heme biosynthesis, *Structure 5*, 1501−1510.
15. Medlock, A., Swartz, L., Dailey, T. A., Dailey, H. A., and Lanzilotta, W. N. (2007) Substrate interactions with human ferrochelatase, *Proc. Natl. Acad. Sci. U.S.A. 104*, 1789−1793.
16. Lecerof, D., Fodje, M., Hansson, A., Hansson, M., and Al Karadaghi, S. (2000) Structural and mechanistic basis of porphyrin metallation by ferrochelatase, *J. Mol. Biol. 297*, 221−232.
17. Gora, M., Grzybowska, E., Rytka, J., and Labbe-Bois, R. (1996) Probing the active-site residues in *Saccharomyces cerevisiae* ferrochelatase by directed mutagenesis. In vivo and in vitro analyses, *J. Biol. Chem. 271*, 11810−11816.
18. Al-Karadaghi, S., Franco, R., Hansson, M., Shelnutt, J. A., Isaya, G., and Ferreira, G. C. (2006) Chelatases: Distort to select? *Trends Biochem. Sci. 31*, 135−142.

19. Dailey, H. A., and Dailey, T. A. (2003) Ferrochelatase, in *The Porphyrin Handbook* (Kadish, K. M., Smith, K. M., and Guildard, R., Eds.) pp 87−114, Elsevier Science, New York.
20. Koch, M., Breithaupt, C., Kiefersauer, R., Freigang, J., Huber, R., and Messerschmidt, A. (2004) Crystal structure of protoporphyrinogen IX oxidase: A key enzyme in haem and chlorophyll biosynthesis, *EMBO J. 23*, 1720−1728.
21. Proulx, K. L., Woodard, S. I., and Dailey, H. A. (1993) In situ conversion of coproporphyrinogen to heme by murine mitochondria: Terminal steps of the heme biosynthetic pathway, *Protein Sci. 2*, 1092−1098.
22. Lange, H., Kispal, G., and Lill, R. (1999) Mechanism of Iron Transport to the Site of Heme Synthesis inside Yeast Mitochondria, *J. Biol. Chem. 274*, 18989−18996.
23. Shaw, G. C., Cope, J. J., Li, L., Corson, K., Hersey, C., Ackermann, G. E., Gwynn, B., Lambert, A. J., Wingert, R. A., Traver, D., Trede, N. S., Barut, B. A., Zhou, Y., Minet, E., Donovan, A., Brownlie, A., Balzan, R., Weiss, M. J., Peters, L. L., Kaplan, J., Zon, L. I., and Paw, B. H. (2006) Mitoferrin is essential for erythroid iron assimilation, *Nature 440*, 96−100.
24. Yoon, T., and Cowan, J. A. (2004) Frataxin-mediated iron delivery to ferrochelatase in the final step of heme biosynthesis, *J. Biol. Chem. 279*, 25943−25946.
25. Shen, Y., and Ryde, U. (2005) Reaction mechanism of porphyrin metallation studied by theoretical methods, *Chemistry 11*, 1549−1564.
26. Sigfridsson, E., and Ryde, U. (2003) The importance of porphyrin distortions for the ferrochelatase reaction, *J. Biol. Inorg. Chem. 8*, 273−282.
27. Shi, Z., and Ferreira, G. C. (2006) Modulation of inhibition of ferrochelatase by N-methylprotoporphyrin, *Biochem. J. 399*, 21−28.
28. Burden, A. E., Wu, C., Dailey, T. A., Busch, J. L., Dhawan, I. K., Rose, J. P., Wang, B., and Dailey, H. A. (1999) Human ferrochelatase: Crystallization, characterization of the [2Fe-2S] cluster and determination that the enzyme is a homodimer, *Biochim. Biophys. Acta 1435*, 191−197.
29. Porra, R. J., Vitols, K. S., Labbe, R. F., and Newton, N. A. (1967) Studies on ferrochelatase. The effects of thiols and other factors on the determination of activity, *Biochem. J. 104*, 321−327.
30. Bender, M. L., Begue-Canton, M. L., Blakeley, R. L., Brubacher, L. J., Feder, J., Gunter, C. R., Kezdy, F. J., Killheffer, J. V., Jr., Marshall, T. H., Miller, C. G., Roeske, R. W., and Stoops, J. K. (1966) The determination of the concentration of hydrolytic enzyme solutions: α-Chymotrypsin, trypsin, papain, elastase, subtilisin, and acetylcholinesterase, *J. Am. Chem. Soc. 88*, 5890−5913.
31. Franco, R., Ma, J. G., Lu, Y., Ferreira, G. C., and Shelnutt, J. A. (2000) Porphyrin interactions with wild-type and mutant mouse ferrochelatase, *Biochemistry 39*, 2517−2529.
32. Fersht, A. R. (1999) *Structure and mechanism in protein science: A guide to enzyme catalysis and protein folding*, Freeman, New York.
33. Franco, R., Bai, G., Prosinecki, V., Abrunhosa, F., Ferreira, G. C., and Bastos, M. (2005) Porphyrin-substrate binding to murine ferrochelatase: Effect on the thermal stability of the enzyme, *Biochem. J. 386*, 599−605.
34. Karlberg, T., Lecerof, D., Gora, M., Silvegren, G., Labbe-Bois, R., Hansson, M., and Al Karadaghi, S. (2002) Metal Binding to *Saccharomyces cerevisiae* Ferrochelatase, *Biochemistry 41*, 13499−13506.
35. Hansson, M. D., Karlberg, T., Rahardja, M. A., Al-Karadaghi, S., and Hansson, M. (2007) Amino Acid Residues His183 and Glu264 in *Bacillus subtilis* Ferrochelatase Direct and Facilitate the Insertion of Metal Ion into Protoporphyrin IX, *Biochemistry 46*, 87−94.

BI602418E